

## Analytical Calculation of the Equivalent Circuit Parameters of Non-Salient Pole Large Synchronous Generators

H. Gorginpour\*

Department of Intelligent Systems Engineering and Data Science, Persian Gulf University, Bushehr, Iran.

**Abstract-** Optimal Design of electrical machines using population-based optimization algorithms needs computationally fast model for evaluating the performance characteristics from design data, i.e. geometric dimensions, winding layouts, material properties. The Electric Equivalent Circuit (EEC) is a simple and appropriate model with acceptable accuracy to be incorporated in the design procedure. In this paper, an analytical approach is presented for calculating the EEC parameters of large non-salient pole synchronous generator based on winding-function method. Although the synchronous generator is well recognized, calculation of its dynamic EEC parameters is not reported in previous studies. Special issues of high-rated industrial synchronous generators are considered such as rotor slots with different dimensions, rotor sub-slots, the damper winding which is created from rotor wedges and retaining rings, saturation of magnetic flux routes in  $d$ - $q$ -axis and stator core stacking. The connections of damper windings in  $d$ - $q$ -axis and definitions of turn-ratios to refer the parameters to the stator-winding side are of novelties of the research. The calculated parameters for a 200MVA power-plant generator are compared with the experimentally obtained parameters. The results of EEC analysis of the studied machine have acceptable coincidence with the experimental and 2D finite-element simulation results, which proves the validity of the proposed method.

**Keyword:** Electric equivalent circuit parameters, Large synchronous generator, Winding-function method.

### NOMENCLATURE

$A_{cf}$	Cross section area of field conductor	$L_{ds}$	Unsaturated $d$ -axis synchronous, transient, sub-transient inductances, respectively
$A_{cs}$	Cross section area of Roebel bar	$L_d', L_d''$	
$B$	Magnetic flux density	$L_q, L_q''$	Unsaturated $q$ -axis synchronous and sub-transient inductances, respectively
$D_{ro}$	Rotor outer diameter	$l_{rd}$	Number of axial cooling ducts
$D_{si}$	Stator inner diameter	$l_{tot}$	Total stator active length
$D_{so}$	Stator outer diameter	$N_{cfx}$	Number of conductors/coil of field winding in $x$ -type slots, $x= A, B, C$
$f_s$	Nominal frequency	$N_{cs}$	Number of stator conductors/coil
$g$	Physical air-gap length	$n_{PB}$	Number of stator winding parallel branches
$H$	Magnetic flux intensity	$N_{rd}$	Number of radial cooling ducts
$h_{rs-sub}$	Height of rotor sub-slots	$N_{rs}$	Total number of rotor slots
$h_{rsx}$	Height of rotor slot of $x$ -type, $x= A, B, C$	$N_{rsx}$	Number of rotor slots of $x$ -type, $x=A, B, C$
$h_{s0}$	Stator wedge thickness+inductance distance	$N_{ss}$	Number of stator slots
$h_{ss}$	Stator slot height	$n_{swl}$	Number of stator winding layers
$h_{sy}$	Stator yoke thickness	$P$	Number of pole pairs
$k_{fe}$	Laminated core stacking factor	$T_a$	DC time constant of stator winding at 75°C
$L_2$	Negative sequence inductance	$T_d'$	$d$ -axis short circuit transient time constant
$L_{dv}$	Saturated $d$ -axis synchronous inductance	$T_d''$	$d$ -axis short circuit sub-transient time constant
$l_{fel}$	Length of one stack of stator core	$T_{do}'$	$d$ -axis open circuit transient time constant
		$T_{do}''$	$d$ -axis open circuit sub-transient time constant
		$T_q''$	$q$ -axis short circuit sub-transient time constant
		$T_{qo}''$	$q$ -axis open circuit sub-transient time constant
		$t_{ring}$	Retaining-ring thickness
		$w_{rs-sub}$	Width of rotor sub-slots
		$w_{rsx}$	Width of rotor slot of $x$ -type, $x= A, B, C$
		$w_{ss}$	Width of stator slot

Received: 20 Dec. 2020

Revised: 21 Jan. 2021

Accepted: 11 Feb. 2021

\*Corresponding author:

E-mail: [h\\_gorgin@pgu.ac.ir](mailto:h_gorgin@pgu.ac.ir) (H. Gorginpour)

DOI: 10.22098/joape.2021.8397.1582

**Research Paper**

© 2021 University of Mohaghegh Ardabili. All rights reserved.

## 1. INTRODUCTION

Large cylindrical-rotor Synchronous Generators (SGs) are widely used as the major power sources in electric-grids. Optimal design of electrical machines using population-based optimization methods needs computationally fast analytical models for predicting the machine performance [1]. The best model, from this point of view, is the dq Electric Equivalent Circuit (EEC) model. The EEC structure in order to model different stator and rotor windings in d- and q- axes are studied in several references, e.g. [2, 3]. The most crucial part of using EEC model in the design procedure is calculation of the circuit parameters with acceptable accuracy knowing the design data, i.e. geometric dimensions, material properties and winding layouts.

The literature review of previous works reveals that the available approaches for parameter estimation of SGs include test procedures, analytical and numerical methods.

The approximate values of d-q-axis equivalent circuit parameters of a SG can be obtained from slip test [4], short circuit test [4, 5], load rejection test [6], standstill and online frequency response tests [4, 7-9] and also, novel methods which get their required data from real time operating tests such as the methods presented in Refs. [10] and [11]. In Ref. [12], the results of the Finite Element (FE) simulations are reported to be in good agreement with the measured results for the EEC parameters. An analytical approach is presented in Ref. [13] for predicting the behavior of salient-pole synchronous machine with no damper winding which calculates the parameters from design data. The application of radial basis neural networks to the development of a novel analytical method for the condition monitoring and fault diagnosis of SGs is studied in Ref. [14]. The general expressions for d- and q- axes inductances of the shorted part of winding are derived using Winding Function (WF) approach considering localized core saturation and then the parameters are determined from the step response test. A non-linear model for SGs using wavelet transform is proposed in Ref. [15] and the results of the identified model show good accuracy comparing the experimental results.

In this paper, an analytical procedure is presented for determining the dq-axis parameters of the large non-salient pole SGs. The motivation of this research is a significant lack of calculation of EEC parameters of power-plant SGs in the literatures that are supported by hardware experiments. Although the WF method is well

recognized in determination of EEC parameter values, its application and definitions of winding layouts in d- and q- axis directions according to the special structure of large SGs, were not established previously. In this study, the special aspects of the power plant generators are considered including rotor slots with different dimensions, rotor sub-slots, damper winding created from rotor wedges and retaining rings, magnetic saturation, stator core stacking, spatial harmonics of windings fields and end-winding effects.

The novelties of the research, which are not reported in previous works, are (a) definitions of damper winding layouts for creating its related *d*- and *q*- axis windings, (b) definitions of turn-ratios for referring the parameters of field and damper winding to stator winding, (c) definitions of Carter's factors for modifying the air-gap length in *d*- and *q*- axis directions, (d) analytical relations for calculating the resistances and leakage inductances of field and damper windings accounting the special forms of end portions of these windings and (e) calculation of saturation factor and MMF drops in different parts of the structure.

In the following, the structure of a large non-salient pole synchronous generator is presented in Section 2. The basic principles of the winding function method is reviewed in Section 3. Then, the analytical procedures of calculating stator, field and damper windings inductances based on the definitions of their related winding functions are given in Section 4. Finally, the results of the EEC parameters of a 200MVA power-plant generator are obtained using analytical, finite-element and experimental methods in Section 5 in order to validate the accuracy of the proposed approach.

## 2. LARGE NON-SALIENT POLE SYNCHRONOUS GENERATOR

### 2.1. Structure

2D cross section of a high-rated power-plant SG with cylindrical rotor is shown in Fig. 1. The stator core carries a 3-phase, 2-layer and short-pitched distributed winding. Each winding conductor is made of insulated and twisted strands, which is called ROEBEL bar. The strands of a conductor can be shorted at both ends using a C-shape piece of copper in order to connect the bars or welding the strands of two bars one by one to each other. It should be noted that the circulating current loss of strands are different for these connecting methods. The stator slots are closed by fiberglass wedges that only play mechanical role of keeping in place the winding conductors. While, the rotor wedges are made from copper alloy, e.g. CuNi2Si+Zr with the

conductivity of  $15 \times 10^6$  Siemens-per-m, and create electrical circuits in addition to mechanically bearing the radial magnetic forces on the field conductors. The rotor wedge bars are short-circuited from both ends via the non-magnetic steel retaining rings. The retaining rings cover the field end-windings. The rotor wedge bars and retaining rings create a damper winding that is a special form of the squirrel cage winding [16]. Hence, there is an induction machine inside the synchronous machine and its resulting torque acts to damp the speed oscillations and to stabilize the operating speed at synchronous speed.

Sub-slots are designed at the bottom of the rotor slots in order to flow of cooling fluid and heat removal. The width of sub-slots should be less than the width of slots for preventing from high saturation level because of narrow flux route in this region. Also, rotor slots with different dimensions are considered in rotor for creating more sinusoidal waveform of field winding flux density. These slots are named A, B and C types as shown in Fig. 1. The radial cooling ducts, which have 5mm-10mm axial length, are inserted between the stator core stacks of about 40mm thickness. The air is used as the cooling fluid for the ratings up to 300MVA and the cooling fluids are  $H_2$  and both  $H_2$  and  $H_2O$  for ratings up to 1000MVA and greater, respectively. The inner diameters of stator core stacks are increased in several steps at both ends in order to reduce the eddy current power loss in these regions, which is due to the end-flux leakage.

**2.2. Equivalent Circuit**

One of the more applicable EEC for analyzing the SG dynamic operational characteristics as per IEEE Std 1110 is depicted in Fig. 2 [17]. In this figure,  $R_s$  and  $L_{ls}$  are the stator resistance and leakage inductance, respectively,  $L_m$  is the magnetizing inductances,  $R_{fd}$  and  $L_{fd}$  are the field winding resistance and leakage inductances, respectively and  $R_D$  and  $L_{Dd}$  are the damper winding resistance and leakage inductance, respectively. In these circuits, all of the parameters are in per-unit form and referred to the stator winding side.

The induced eddy current in the rotor pole faces, due to the spatial harmonics of rotating magnetic field, can be modeled as a damper-winding branch in q-axis EEC model. The parameters of the winding, which models this phenomenon, are commonly exploited by fitting curves on the test results. This damper-winding is not considered in this research. Also, there is a coupling inductance in the modified d-axis EEC for accounting the phenomenon of increased flux linkage between damper and field windings. Insertion of this inductance

and modifying the values of  $L_{fd}$  and  $L_{Dd}$  cause negligible effect on the stator side parameters and behaviors while big error in the calculation of field winding sub-transient induced current [8]. Again, this inductance is not included in this study. However, the models of Fig. 2 introduce acceptable accuracy for most transient and dynamic analyses. In the future works, the analytical calculations of damper-winding modelling the eddy currents in the rotor pole faces and the coupling reactance reported in Ref. [8] can be pursued.

In this paper, an analytical approach for estimating the parameter values of the EEC model of Fig. 2 is presented. The main features of the proposed approach that makes it suitable for large generators includes:

- Considering special structure of stator slot in calculation of stator winding leakage reactance.
- Considering rotor slots with different dimensions, i.e. A, B and C slot types, and sub-slots in calculation of field and damper windings parameters.
- Considering the effect of radial cooling ducts on the calculation of effective axial length. It should be noted that the axial length is a key parameter for calculation of all of the EEC parameters.
- Considering the damper winding as a winding created from the rotor wedge bars and the retaining rings.
- Considering the especial forms of the end-windings in calculation of leakage reactances.

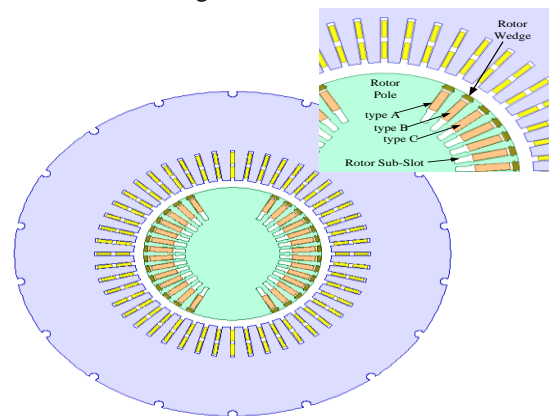


**Fig. 1. 2D cross section of large non-salient pole SG**

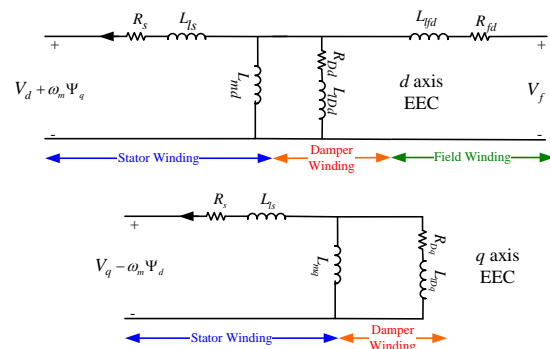


**Fig. 2. d- and q- axes EEC of SG**

### 2.3. Required Parameters

After calculating the EEC parameters, the additional parameters and time constants that are required in dynamic analyses can be obtained as follows [3],

$$L_d = L_{md} + L_{ls} \quad (1)$$

$$L_{dv} = k_{at} L_{md} + L_{ls} \quad (2)$$

$$SCR = 1 / (2\pi f_s L_{dv}) \quad (3)$$

$$L'_d = L_{ls} + L_{md} L_{lfd} / (L_{md} + L_{lfd}) \quad (4)$$

$$L''_d = L_{ls} + L_{md} L_{lfd} L_{lDd} / (L_{md} L_{lfd} + L_{md} L_{lDd} + L_{lfd} L_{lDd}) \quad (5)$$

$$L_q = L'_q = L_{mq} + L_{ls} \quad (6)$$

$$L''_q = L_{ls} + L_{mq} L_{lDq} / (L_{mq} + L_{lDq}) \quad (7)$$

$$T'_{do} = (L_{md} + L_{lfd}) / R_{fd} \quad (8)$$

$$T''_{do} = [L_{lDd} + L_{md} L_{lfd} / (L_{md} + L_{lfd})] / R_{Dd} \quad (9)$$

$$T'_d = T'_{do} L'_d / L_d \quad (10)$$

$$T''_d = T''_{do} L''_d / L_d \quad (11)$$

$$T''_{qo} = (L_{mq} + L_{lDq}) / R_{Dq} \quad (12)$$

$$T''_q = T''_{qo} L''_q / L_q \quad (13)$$

$$L_2 = 0.5(L''_d + L''_q) \quad (14)$$

$$T_a = L_2 / R_{s@75^\circ C} \quad (15)$$

It should be noted that all of these inductances are in per-unit and their related reactance values are obtained by multiplying into  $2\pi f_s$ . It is assumed that only the magnetizing inductance is saturable and thus the saturated value of this inductance should be used in order to calculate the saturated values of Eqns. (4)-(15).

### 3. WINDING FUNCTION METHOD

The WF method is used successfully for calculation of inductances of different electric machines such as induction machine, synchronous machine, and permanent magnet machines [18-22].

The analytical relations of self-inductance of  $i^{th}$  winding and mutual inductance between  $i^{th}$  and  $j^{th}$  windings are as Eqns. (16) and (17), respectively [19].

$$L_{ii} = \frac{\mu_0 D_{ag} l_{eff}}{2gn_{PB}} \int_0^{2\pi} n_i(\theta) N_i(\theta) d\theta \quad (16)$$

$$L_{ij} = \frac{\mu_0 D_{ag} l_{eff}}{2gn_{PB}} \int_0^{2\pi} n_j(\theta) N_i(\theta) d\theta \quad (17)$$

where  $l_{eff}$  is the effective stack length and can be evaluated using Eqns. (18) and (19), respectively [23].  $n(\theta)$  and  $N(\theta)$  are Turn Function (TF) and Winding Function (WF), respectively.

$$l_{eff} = l_{tot} (1_{fe1} + 1_{rd} - 0.5g\xi) / (1_{fe1} + 1_{rd}) \quad (18)$$

$$\xi = \frac{2}{\pi} [2l_{rd} / g \tan^{-1}(l_{rd} / g) - \ln(1 + (l_{rd} / g)^2)] \quad (19)$$

The relation between TF and WF functions is Eq. (20). In fact, WF is the ac component of TF in the case of uniform air-gap length [19].

$$N(\theta) = n(\theta) - \langle n(\theta) \rangle \quad (20)$$

where  $\langle n(\theta) \rangle$  is the average component of the turn function.

The mutual inductance between two windings, which are stationary regarding to each other, is a constant value. While, the mutual inductances between the stator windings and rotor windings are functions of the rotor angular position. Some assumptions are considered in the WF method: (a) the magnetic permeability of stator and rotor cores is infinite, (b) the magnetic flux lines cross the air-gap region in parallel and the fringing flux at the core ends is ignored, (c) the effect of stator and rotor core slotting can be considered by applying Carter's factor, (d) the effect of stator core stacking can be addressed by defining axial Carter's factor.

The WF of the stator winding of the studied generator is shown in Fig. 3, which is 3-phase, 2-pole, distributed in 60 slots, double-layers with 5/6 short pitched and 1 conductor-per-turn. As it can be seen, the variations are not step like but the function value is assumed to be linearly varied over the slot width.

## 4. CALCULATING THE EEC INDUCTANCES

### 4.1. Stator Winding Inductances

The magnetic flux and turn functions of one stator coil are depicted in Fig. 4 (a) and (b), respectively. In this figure,  $B_{1sd}$  and  $B_{2sd}$  are evaluated as Eqns. (21) and (22).

$$B_{1sd} = \mu_0 N_{cs} (-\frac{\alpha_{sc}}{2\pi}) / g_{eff,d} \quad (21)$$

$$B_{2sd} = \mu_0 N_{cs} (1 - \frac{\alpha_{sc}}{2\pi}) / g_{eff,d} \quad (22)$$

where  $g_{eff,d}$  is the  $d$ -axis effective air-gap length which can be calculated using Eqns. (23) and (24). The correction factor of calculating effective air-gap length is in fact the Carter's factor. Ref. [23] gives comprehensive details on definition and mathematical relation of Carter's factor.

$$g_{eff,d} = g \frac{\pi D_{si}}{\pi D_{si} - g N_{ss} \xi_s} \quad (23)$$

$$\xi_s = \frac{2}{\pi} [2w_{ss} / g \tan^{-1}(w_{ss} / (2g)) - \ln(1 + (w_{ss} / (2g))^2)] \quad (24)$$

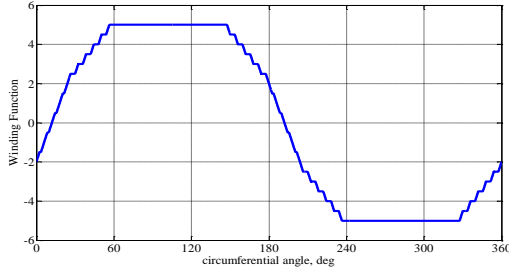


Fig. 3. WF of one stator phase winding of the studied generator

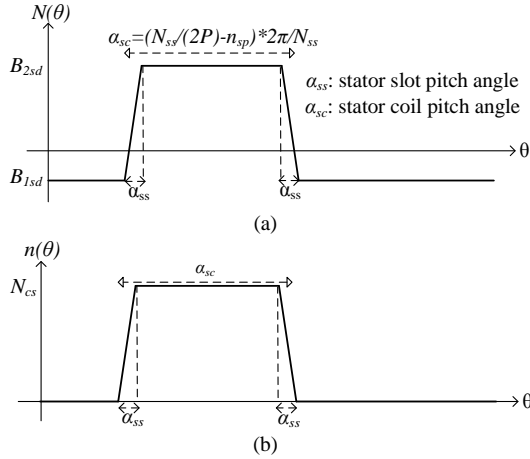


Fig. 4. (a) Winding function and (b) turn function of a single stator coil

There is no rotor slot in  $d$ -axis. Hence, only the stator Carter's factor is used in the relation of  $g_{eff,d}$ . It should be noted that the following procedure is the same for the  $q$ -axis except of the effective air-gap length in this direction.  $g_{eff,q}$  is larger than  $g_{eff,d}$  because of the presence of the rotor slots in the  $q$ -axis region. Hence, the  $g_{eff,q}$  is calculated using (25) considering rotor Carter's factor.

$$g_{eff,q} = g_{eff,d} \tau_{rs} / (\tau_{rs} - \xi_r g) \quad (25)$$

where  $\tau_{rs}$  is the rotor slot pitch length which is practically chosen the same for  $A$ ,  $B$  and  $C$  slot types, and the relation of  $\xi_r$  can be written using (24) by substituting  $w_{rs}$  instead of  $w_{ss}$ .

The flux and turn functions are created for all of the winding coils by shifting the base functions that are created for the reference angle. These two functions are coded as two matrices in the numerical analytic program. Each row of the  $0.5N_{ss}$  rows matrix for single-layer winding and  $N_{ss}$  rows matrix for double-layer winding, is related to a winding coil. The column number of the matrices should be selected so that the functions variations could be seen smoothly and the numerical integrations could be evaluated precisely. In addition, the column number must be an integer factor of the great common divider of the stator and rotor slot numbers.

$$column\ number = k \times gcd\{N_{ss}, round[\max(2\pi/\alpha_{rsx})]\} \quad (26)$$

In fact, each column is related to a mechanical angle

of  $360/(column\ number)$  degree. The second part rows for the double-layers winding matrices are shifted rows of the first part by the column numbers related to  $n_{sp}$ -slots of short-pitching.

Performing numerical integrations on the multiplications of the  $d$ - and  $q$ - axis flux functions by their turn functions yield inductance matrices of  $M_{ssd}$  and  $M_{ssq}$  with  $N_{ss} \times N_{ss}$  dimensions. These matrices contain coils self-inductances and the mutual-inductances between each coil and other coils. The inductance matrices of the stator phase windings are calculated as,

$$L_{ssx} = T \times M_{ssx} \times T^T, \quad x = d, q \quad (27)$$

$T$  is a  $3 \times N_{ss}$  dimension matrix which determines the dependency or independency of each coil to the phase windings and also, the current flow direction. It contains only 0, 1, -1.

$L_{ssx}$  is a  $3 \times 3$  matrix containing the self- and mutual-inductances of phase windings in  $x$ -axis. Using this matrix, the  $d$ - and  $q$ - axis magnetizing inductances, i.e.  $L_{md}$  and  $L_{mq}$ , and zero sequence inductance, i.e.  $L_0$ , can be obtained,

$$L_{aa0} = 0.5(L_{ssd}(1,1) + L_{ssq}(1,1)) \quad (28)$$

$$L_{ab0} = 0.5(L_{ssd}(1,2) + L_{ssq}(1,2)) \quad (29)$$

$$L_{aa2} = 0.5(L_{ssd}(1,1) - L_{ssq}(1,1)) \quad (30)$$

$$L_{md} = L_{aa0} - L_{ab0} + 1.5L_{aa2} \quad (31)$$

$$L_{mq} = L_{aa0} - L_{ab0} - 1.5L_{aa2} \quad (32)$$

$$L_0 = L_{aa0} + 2L_{ab0} \quad (33)$$

The per-unit reactances are calculated by dividing each reactance on the base impedance, i.e. (nominal kV)<sup>2</sup>/(nominal kVA).

In the following, the calculation of stator winding leakage inductance is discussed. The leakage inductance consists the following terms:

1- The differential leakage inductance that models the spatial harmonics of the air-gap magnetic flux. The specific permeance of this term is calculated from the real winding distribution using WF as [23].

$$\lambda_{sh} = \frac{3D_{st}qI_{fe}}{\pi N_{ss}g_{eff}l_{eff}} \left\{ 2\left(\frac{\pi}{3k_{wls}}\right)^2 [5q_s^2 + 1 - 0.125(2.75q_s^2 + 2)] / (12q_s^2) - 1 \right\} \quad (34)$$

2- The slot leakage inductance that models the flux lines closing their routes from hollow slot body. The specific permeance of this term for 2-layers, 5/6 short-pitched winding is Eq. (35) [23]. Fig. 5 shows the stator slot structure and its insulation details. The parameters used in Eq. (35), are indicated in this figure.

$$\lambda_{ss} = 0.9063 \frac{2h_{cs}}{3w_{ss}} + 0.875 \frac{h_{s0}}{w_{ss}} + \frac{z_{ins} + z_{main}}{4w_{ss}} \quad (35)$$

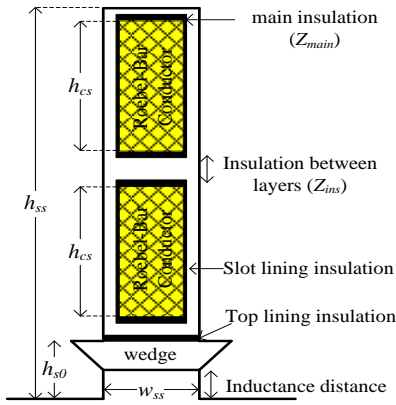


Fig. 5. The stator slot structure and its insulation details

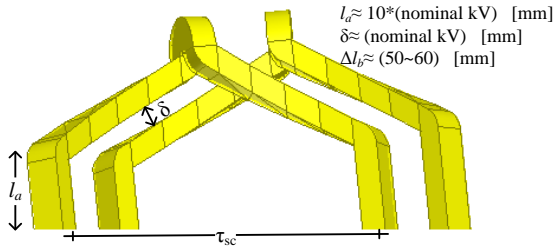


Fig. 6. The end-regions of two adjacent stator coils

3- The zig-zag leakage inductance models the zig-zag flux path between stator and rotor teeth when a stator tooth is opposite to a rotor slot. The related specific permeance is calculated as [23],

$$\lambda_{zz} = \frac{5g_{eff}}{w_{ss}(5+4g_{eff}/w_{ss})} \frac{7}{D_{st}\alpha_{sc}} \quad (36)$$

4- The end-winding leakage inductance due to end regions flux is evaluated as,

$$L_{ew} = 0.21\mu_0 N_{sw}^2 \frac{2l_{ew}}{P} \quad (37)$$

$$l_{ew} = \tau_{sc} \sqrt{1 - (N_{ss}(w_{ss} + \delta) / (\pi D_{st}))^2} + \pi h_{ss} / 4 + 2l_a + \Delta b \quad (38)$$

where  $N_{sw}$  is the number of series turns-per-phase of stator winding,

$$N_{sw} = N_{ss} N_{sc} n_{swl} / (6n_{PB}) \quad (39)$$

The geometrical parameters for calculating the end-winding length are graphically shown in Fig. 6. Finally, the stator leakage inductance in H unit is calculated using Eq. (40).

$$L_{ls} = 12\mu_0 N_{sw}^2 l_{fe} (\lambda_{sh} + \lambda_{ss} + \lambda_{zz}) / N_{ss} + L_{ew} \quad (40)$$

#### 4.2. Field Winding Inductance

The FW generates a static magnetic flux only in the d-axis direction. The connection layout of a 2-pole FW is shown in Fig. 7. Hence, there are  $N_{rs}/(4P)$  different coil-pitch angles which is named as  $\alpha_{fck}$  ( $k=1: N_{rs}/(4P)$ ).

The TF and WF matrices are created for all coils located in A, B and C slot types. In these matrices with

$(0.5N_{rs} \times \text{column number})$  dimension, each row is related to one coil. In creation of flux function for each coil, as same as Fig. 4(a), the lower and upper values of magnetic field, which depend on the coil span and the slot type, can be obtained using Eqns. (41) and (42), respectively.

$$B_{1fk} = \frac{\mu_0 N_{cfk}}{g_{eff,q}} \left( -\frac{\alpha_{fck}}{2\pi} \right), k=1: \frac{N_{rs}}{4P}, x: A, B, C \quad (41)$$

$$B_{2fk} = \frac{\mu_0 N_{cfk}}{g_{eff,q}} \left( 1 - \frac{\alpha_{fck}}{2\pi} \right), k=1: \frac{N_{rs}}{4P}, x: A, B, C \quad (42)$$

It should be noted that the effective air-gap length in the rotor slot locations is  $g_{eff,q}$ . Because of series connection between FW coils, the rows of the TF and WF matrices are summed together and two vectors with *column number* length are resulted. The WF distribution of the FW of the studied generator is depicted in Fig. 8.

The FW self-inductance value ( $M_{ff}$ ) is calculated using Eq. (16). The mentioned procedure is repeated in order to obtain the fundamental component of self-inductance ( $M_{ff1}$ ) from the fundamental component distributions of TF and WF. The difference between  $M_{ff}$  and  $M_{ff1}$  is the leakage inductance due to the magnetic field spatial harmonics ( $M_{ffn}$ ). In the following, the base value of FW inductance referred to the stator side is,

$$L_{fd,B} = \frac{M_{ff1} \ddot{u}_f^2}{L_{md}} \quad (43)$$

where  $\ddot{u}_f$  is the turn-ratio between stator and field windings. The turn ratio of two windings is defined as the ratio between the fundamental component amplitudes of their related winding functions.

$$\ddot{u}_f = \frac{1.5 |N_{a1}(\theta)|}{|N_{f1}(\theta)|} \quad (44)$$

where  $|N_{a1}(\theta)|$  and  $|N_{f1}(\theta)|$  are the amplitudes of the fundamental component distributions of WFs of the stator and field windings.

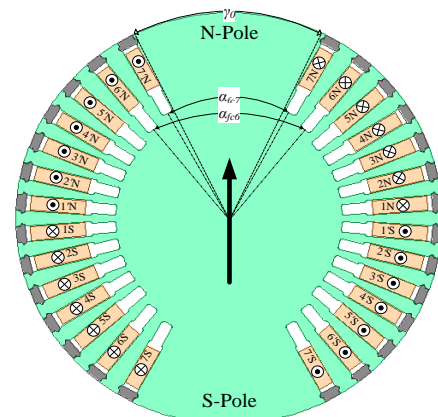


Fig. 7. Connection layout of a 2-pole FW

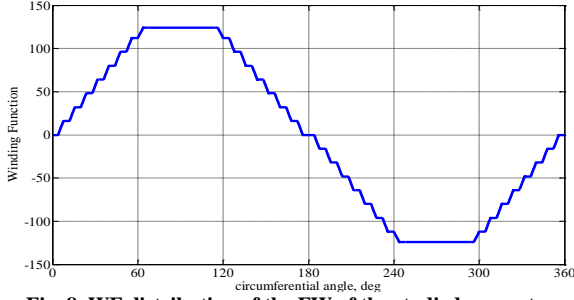


Fig. 8. WF distribution of the FW of the studied generator

The per-unit and referred FW leakage inductance, i.e.  $L_{lfd}$ , is evaluated in (45)-(48) with neglecting the zig-zag leakage inductance,

$$L_{lfd} = \frac{L_f \dot{u}_f^2}{L_{fd,B}} \quad (45)$$

$$L_f = M_{fjh} + \sum_{x:A,B,C} N_{rsx} N_{cfx}^2 [\lambda_{rsx} l_{eff} + 2\lambda_{few} l_{ewx}] \quad (46)$$

where  $l_{ewx}$  is the total end-region length of conductors located in  $x$ -type rotor slots. Also, the slot and end-winding permeances are stated in Eqns. (47) and (48), respectively [23].

$$\lambda_{rsx} = \mu_0 \left( \frac{h_{rsx} - h_{r0w}}{3w_{rsx}} + \frac{h_{r0w}}{w_{rsx}} \right) \quad (47)$$

$$\lambda_{few} \cong 0.34\mu_0 \quad (48)$$

### 4.3. Damper Winding Inductances

The damper winding is a cage winding consists of the wedges as the bars and the retaining rings as the end-rings. The referred per-unit  $dq$  resistances and inductances of this winding are required for creating the EEC. In order to create the  $d$ - and  $q$ - axes WF, the connection layouts between bars through end-rings should be assumed such that the resulting magnetic fields orient in  $d$ - and  $q$ - axes, respectively. The TF and WF matrices are of  $(0.5N_{rs} \times \text{column number})$  dimension and each row is related to a specific coil. In creation of  $d$ -axis WF for each coil, as same as Fig. 4(a), the lower and upper values of magnetic fields depending on the coil span, are calculated using Eqns. (49) and (50), respectively.

$$B_{1Ddk} = \frac{\mu_0}{g_{eff,q}} \left( -\alpha_{Dck} / 2\pi \right), k = 1: \frac{N_{rs}}{4P} \quad (49)$$

$$B_{2Ddk} = \frac{\mu_0}{g_{eff,q}} \left( 1 - \alpha_{Dck} / 2\pi \right), k = 1: \frac{N_{rs}}{4P} \quad (50)$$

where  $\alpha_{Dck}$  is the  $k^{\text{th}}$  DW coil angle which generates magnetic flux in  $d$ -axis direction. These angles are the same as  $\alpha_{fck}$  angles in Fig. 7. These relations for the  $q$ -axis WF of coils are the same except for the coil span angles. The rows of TF and WF of  $d$ - and  $q$ - axes are summed together and two vectors with  $(\text{column number})$  length are resulted for each axis. The magnetic flux

spatial distributions of damper winding of the studied generator in  $d$ - and  $q$ - axes are depicted in Fig. 9. These distributions are the same as the WF distributions except for their magnitudes.

The DW self-inductance values, i.e.  $M_{DdDd}$  and  $M_{DqDq}$ , are calculated using Eq. (16). Also, the fundamental components of self-inductances, i.e.  $M_{DdDd1}$  and  $M_{DqDq1}$ , are obtained from the fundamental component distributions of TF and WF. The differences between these inductances are the leakage inductances due to the magnetic field spatial harmonics, i.e.  $M_{DdDdh}$  and  $M_{DqDqh}$ . The base value of  $d$ -axis DW inductance referred to the stator winding side is,

$$L_{dD,B} = \frac{M_{DdDd1} \dot{u}_{Dd}^2}{L_{md}} \quad (51)$$

where  $\dot{u}_{Dd}$  is the turn ratio between stator winding and  $d$ -axis damper winding,

$$\dot{u}_{Dd} = \frac{1.5 |N_{d1}(\theta)|}{|N_{Dd1}(\theta)|} \quad (52)$$

where  $|N_{Dd1}(\theta)|$  is the amplitude of the fundamental component of WF distribution of the  $d$ -axis damper winding. Similarly, the  $q$ -axis base value of DW inductance referred to the stator side can be concluded.

The mutual inductances between DW loops are not included in calculation of leakage inductance. Also, the zig-zag flux leakage is assumed negligible. The per-unit and referred  $d$ -axis damper winding leakage inductance, i.e.  $L_{lDd}$ , is evaluated as,

$$L_{lDd} = \frac{L_{lDdDd} \dot{u}_{Dd}^2}{L_{Dd,B}} \quad (53)$$

$$L_{lDdDd} = 2N_{rs} l_{tot} \lambda_{rw} + 4l_{ring,d} \lambda_{ring} \quad (54)$$

$$\lambda_{rw} = \frac{h_{rw}}{3w_{rs}} \quad (55)$$

$$\lambda_{ring} \cong 0.2\mu_0 \quad (56)$$

where  $l_{ring-d}$  is the sum of current paths between wedge bars through retaining-rings in such a way that create  $d$ -axis direction magnetic field.

$$l_{ring,d} = 0.5(D_{ro} - t_{ring}) \sum_{k=1}^{N_{rs}/2} \alpha_{Dck} \quad (57)$$

In the case of calculating  $q$ -axis quantities, the connections between wedge bars are chosen so that the resulting loops create magnetic field in this direction.

Contrary to that may be viewed from Fig. 9. The  $d$ -axis flux distribution is more sinusoidal than that of  $q$ -axis. This can be concluded from the spatial harmonic components of  $d$ - and  $q$ - axis flux distributions shown in Fig. 10.

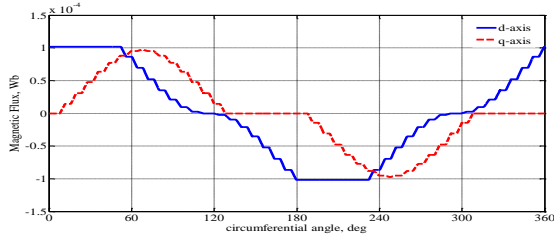


Fig. 9. The magnetic flux functions of the studied generator in  $d$ - and  $q$ - axes

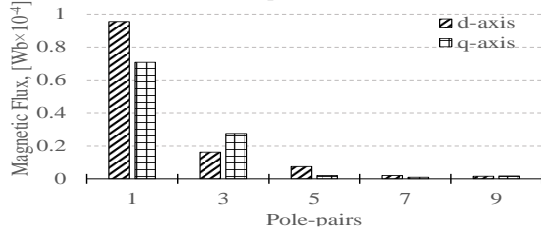


Fig. 10. Spatial harmonic components of magnetic flux distributions of Fig. 9

#### 4.4. Saturation

The calculation of Saturation Factor ( $k_{sat}$ ), which indicates the level of iron-core magnetic saturation, is discussed in this subsection. The Magneto-Motive Forces (MMFs) in different parts of the magnetic flux route and different no-load terminal voltage magnitudes should be determined at first. The relation of total flux per pole ( $\Phi_p$ ) is,

$$\Phi_p = (\pi B_{av} D_{si} l_{eff}) / (2P) \quad (58)$$

where  $B_{av}$  is the average air-gap magnetic flux density or magnetic loading which is obtained from the overall machine electromagnetic utilization and the current loading. The following relations can be evaluated for each terminal voltage magnitude ( $V_{t,pu}$ ) from 0pu up to 1.4pu in discretized steps.

- The air-gap MMF drop ( $\Psi_{ag}$ ):

$$\Psi_{ag} = \frac{\pi}{2\mu_0} V_{t,pu} B_{av} g_{eff,q} \quad (59)$$

- The stator tooth MMF drop ( $\Psi_{st}$ ):

$$B_{st} = \pi V_{t,pu} \Phi_p / (h_{st} \frac{1}{3} l_{fe} k_{fe} N_{ss} / P) \quad (60)$$

$$h_{st} \frac{1}{3} = \pi (D_{si} + 2h_{ss} / 3) / N_{ss} - w_{ss} \quad (61)$$

From the stator core B-H curve  $\rightarrow H_{st}$

$$\Psi_{st} = H_{st} h_{ss} \quad (62)$$

- The stator yoke MMF drop ( $\Psi_{sy}$ ):

$$B_{sy} = 0.5\pi V_{t,pu} \Phi_p / (h_{sy} l_{fe} k_{fe}) \quad (63)$$

From the stator core B-H curve  $\rightarrow H_{sy}$

$$\Psi_{sy} = \frac{\pi}{2} H_{sy} (D_{so} - h_{sy}) / (2P) \quad (64)$$

- The rotor pole face MMF drop ( $\Psi_{rp}$ ):

$$B_{rp} = V_{t,pu} \Phi_p / \{0.51 l_{tot} [\gamma_0 (D_{ro} - \frac{2}{3} (h_{rsa} + h_{rs-sub}))]\} \quad (65)$$

From the stator core B-H curve  $\rightarrow H_{rp}$

$$\Psi_{rp} = H_{rp} (h_{rsa} + h_{rs-sub}) \quad (66)$$

-The rotor pole-face MMF drop ( $\Psi_{ry}$ ):

$$B_{ry} = V_{t,pu} \Phi_p / \{0.5\pi l_{tot} (D_{ro} - 2(h_{rsa} + h_{rs-sub}))\} \quad (67)$$

From the rotor forge B-H curve  $\rightarrow H_{ry}$

$$\Psi_{ry} = 0.5 H_{ry} (D_{ro} - 2(h_{rsa} + h_{rs-sub})) \quad (68)$$

The total MMF drop in flux route ( $\Psi_{tot}$ ) is,

$$\Psi_{tot} = \Psi_{ag} + \Psi_{st} + \Psi_{sy} + \Psi_{rp} + \Psi_{ry} \quad (69)$$

The field current for inducing the terminal voltage under open-circuit condition ( $I_{fOCC}$ ) can be calculated using Eq. (70).

$$I_{fOCC} = \Psi_{tot} / (4P \sum_{x:A,B,C} N_{rsx} N_{cfx}) \quad (70)$$

The required field current in order to generate nominal terminal voltage ( $I_{f,ni}$ ) is obtained from these relations considering  $V_{t,pu}$  to 1pu. The MMF drop due to load current ( $I_s$ ) and its related armature reaction is as,

$$\Psi_{ar} = 1.35 N_s k_{wls} I_s / P \quad (71)$$

The required field current for developing stator field and compensating armature reaction is as Eq. (72). In fact,  $I_{f,sc}$  is the field current for stator current on sustained symmetrical short-circuit.

$$I_{f,sc} = [\Psi_{ar} + 2\pi f_s L_s (\Psi_{ag} |_{V_{t,pu}=1pu})] / (4P \sum_{x:A,B,C} N_{rsx} N_{cfx}) \quad (72)$$

The saturated  $d$ -axis magnetizing reactance of stator winding, i.e.  $X_{dv}$ , is the slope of  $V_{t,pu}$  versus  $I_{f,pu}$  at the (1pu,  $I_{f,sc}$ pu) point.  $k_{sat}$  is the ratio of saturated and unsaturated  $d$ -axis magnetizing reactances of stator winding. Also, the short circuit ratio is vice versa of  $X_{dv}$ .

## 5. RESULTS AND DISCUSSION

The specifications of the studied generator are listed in Table 1. This machine is a 200MVA, 15.75kV, 2-pole and 50Hz power-plant generator. The stator-laminated magnetic core is of M330-50A grade and the rotor forge material is steel 26NiCrMoV14-5 type. The analytical and experimental results of the studied generator under rated loading and 0.8 power-factor are listed in Table 2. According to the last column of this table, the exposed error between analytical and experimental results are in acceptable range of below than 10%. The manufacturer conducts several experiments in order to determine the parameters and operational characteristics.

Table 1. The Specifications of the Studied Generator

Specification	Value	Specification	Value
$D_{ag}$	1220mm	$N_{rsC}$	0
$l_{fe}$	3300mm	$N_{crA}$	16
$N_{ss}$	60	$N_{crB}$	12
$w_{ss}$	25.9mm	$\alpha_{rs}$	$2\pi/45$ rad
$h_{ss}$	254.2mm	$w_{rs}$	39.6mm
$h_{s0}$	16.4mm	$h_{rsa}$	184.8mm
$h_{sy}$	512.8mm	$h_{rsB}$	151.1mm
$N_{cs}$	1	$N_{rd}$	105
$g$	70mm	$l_{rd}$	8mm
$n_{PB}$	2	$h_{rdw}$	31.5mm
$N_{rsa}$	28	$w_{rs-sub}$	30mm
$N_{rsB}$	4	$h_{rs-sub}$	55mm

**Table 2. The Analytical and Experimental Results of the EEC and Other Parameters and Time Constants of the Studied Generator**

Parameter	Analytical Method	Experimental Result	Absolute Error
$X_{dl}$	0.148215 p.u.	0.14634 p.u.	1.28%
$X_{ad}$	1.810049 p.u.	1.839 p.u.	1.57%
$X_d$	1.958264 p.u.	1.978 p.u.	1%
$X_{dv}$	1.740884 p.u.	1.7051 p.u.	2.1%
$X_{dq}$	1.728831 p.u.	1.74 p.u.	0.64%
$X_q$	1.877046 p.u.	1.879 p.u.	0.1%
$X_{fd}$	0.093814 p.u.	0.09394 p.u.	0.13%
$R_{fd}$	0.000514 p.u.	0.0005756 p.u.	10.7%
$X_{Dd}$	0.023560 p.u.	0.02508 p.u.	6.06%
$R_{Dd}$	0.008013 p.u.	0.008101 p.u.	1.08%
$X_{Dq}$	0.034412 p.u.	0.03618 p.u.	4.88%
$R_{Dq}$	0.002926 p.u.	0.002827 p.u.	3.5%
$X_d''$	0.166852 p.u.	0.1586 p.u.	5.2%
$X_d'$	0.237406 p.u.	0.2217 p.u.	7.08%
$X_q''$	0.181955 p.u.	0.1745 p.u.	4.3%
$T_{do}'$	11.791933 s	11.38 s	3.6%
$T_d'$	1.329569 s	1.264 s	5.2%
$T_{do}''$	0.044790 s	0.04224 s	6.3%
$T_d''$	0.031479 s	0.03048 s	3.3%
$T_{qo}''$	1.918214 s	2 s	4.09%
$T_q''$	0.185946 s	0.1928 s	3.5%
$X_2$	0.174404 p.u.	0.1874 p.u.	6.9%
$T_a$	0.446397 s	0.46701 s	4.4%
$X_p$	0.237406 p.u.	0.22145 p.u.	7.2%
SCR	0.574421	0.58648	2.05%
$X_{q0}$	0.089481 p.u.	0.0983 p.u.	8.9%

**Table 3. Comparison between the Experimental Results and the Results of the Analytical and 2D FE Models of the Studied Generator**

Characteristic/Parameter	Experimental	Analytical	2D FE
$I_{f,nl}$	459A	461.8A	448A
$I_{f,sc}$	780A	797.8A	762A
$X_2$	0.1874 p.u.	0.1744 p.u.	0.2099 p.u.
$X_0$	0.0983 p.u.	0.08548 p.u.	0.1123 p.u.
$X_d''$	15.3%	15.17%	24.87%
$X_d'$	24.3%	22.21%	29.7%
$T_d'$	1.431 s	1.3638 s	1.142 s
$T_d''$	0.0362 s	0.0308 s	0.0247 s
$T_a$	0.392 s	0.4183 s	0.4391 s

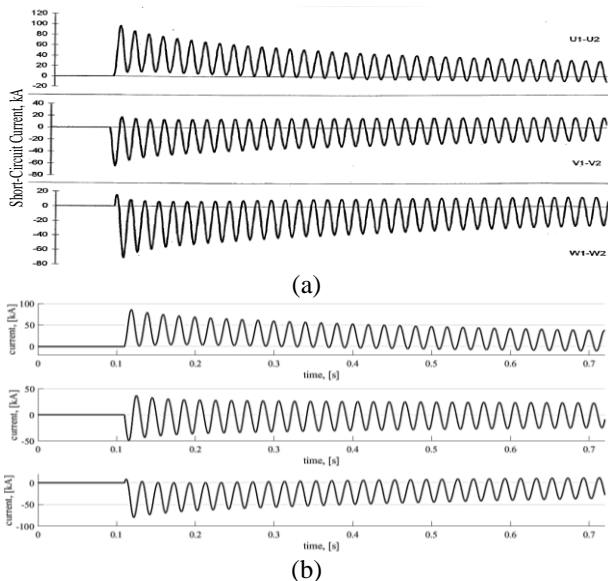


**Fig. 11. The stator phase currents in short-circuit test at 70% rated voltage before test and no-load condition obtained from (a) experimental measurements, (b) simulation in MATLAB/SIMULINK software using dynamic EEC models and analytically calculated parameters given in Table 2**

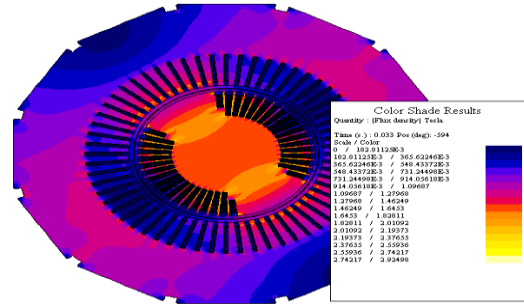


**Fig. 12. 2D magnetic field pattern of the studied generator under rated operating condition**

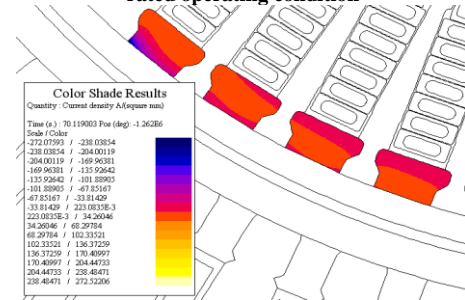


**Fig. 13. The current density distribution in rotor wedge bars in sub-transient period of 3-phase short-circuit condition**

The short-circuit test is the most common and appropriate test for extracting the EEC parameter values. The stator phase currents in short-circuit test at 70% rated voltage before test and no-load condition are shown in Fig. 11(a). The measured waveforms are in good coincidences with the results of simulation in MATLAB/SIMULINK software (Fig. 11(b)) using dynamic EEC models and analytically calculated parameters given in Table II. The results of the zero-sequence reactance test, negative-sequence reactance test, the short-circuit test and other measurements are compared with the analytical and 2D FE results in Table 3. It should be noted that the tests are simulated using FE software and the parameters and time-constants are derived using the methods described in IEEE std 115, IEEE std 1110 and IEC 60034-4. In 2D FE simulations, the winding resistances and the leakage inductance terms related to the third dimension, i.e. end-winding leakage inductance, are inserted in the external circuit attached to the electro-magnetic model. It can be seen that the errors of all parameters fall in acceptable range and thus proves desirable accuracy. Fig. 12 shows the magnetic field density distribution in 2D cross section of the generator under rated operating condition, which is obtained from FE analysis. As it mentioned previously, under sudden short circuit and sub-transient period, the damper winding plays an important role in the dynamic behavior of the machine. This is due to high current amplitude passing through wedge bars. The 2D pattern of current density in rotor wedge bars during sub-transient period of short-circuit phenomenon is illustrated in Fig. 13.

## 6. CONCLUSION

The paper presents analytical procedures for calculating the parameters of  $dq$  electric equivalent circuit of large non-salient pole synchronous generators. The method is based on the winding function approach, which only requires geometrical dimensions, winding layouts and material specifications. Special issues of high-rated industrial synchronous generators are considered such as rotor slots with different dimensions, rotor sub-slots, the damper winding, saturation of magnetic flux route and stator core stacking. The novelties of the research, which are not reported in previous works, are (a) definitions of damper winding layouts for creating its related  $d$ - and  $q$ - axis windings, (b) definitions of turn-ratios for referring the parameters of field and damper winding to stator winding, (c) definitions of Carter's factors for modifying the air-gap length in  $d$ - and  $q$ - axis directions, (d) analytical relations for calculating the resistances and leakage inductances of field and damper windings accounting the special forms of end portions of these windings and (e) calculation of saturation factor and MMF drops in different parts of the structure. The analytical results of EEC parameters of a 200MVA, 2-pole, 50Hz studied generator are compared with the experimental and 2D finite-element results which prove acceptable accuracy and validity of the analytical relations. The presented method can be effectively used in optimal design stage and in collecting required data for dynamic analysis of power network.

## REFERENCES

- [1] H. Gorginpour, "Analysis and design considerations of an axial-flux dual-rotor consequent-pole Vernier-PM machine for direct-drive energy conversion systems", *IET Renew. Power Gener.*, vol. 14, pp. 211-21, 2020.
- [2] D. Aliprantis et al, "A synchronous machine model with saturation and arbitrary rotor network representation", *IEEE Trans. Energy Convers.*, vol. 20, pp. 584-594, 2005.
- [3] T. Lipo, *Analysis of Synchronous Machines*, 2<sup>nd</sup> ed., Florida, CRC Press: Taylor & Francis Group, 2012.
- [4] Test Procedures for Synchronous Machines, IEEE Std. 115, Dec. 1995.
- [5] A. Tassarolo et al., "A new method for determining the leakage inductances of a nine-phase synchronous machine from no-load and short-circuit tests", *IEEE Trans. Energy Convers.*, vol. 30, pp. 1515-27, 2015.
- [6] F. Mello and L. Hannett, "Validation of synchronous machine models and derivation of model parameters from tests", *IEEE Power Eng. Rev.*, vol. 1, pp. 19-20, 1981.
- [7] D. Aliprantis et al., "Experimental characterization procedure for a synchronous machine model with saturation and arbitrary rotor network representation", *IEEE Trans. Energy Convers.*, vol. 20, pp. 595-603, 2005.
- [8] I. Canay, "Determination of the model parameters of machines from the reactance operators  $x_d(p)$ ,  $x_q(p)$ ", *IEEE Trans. Energy Convers.*, vol. 8, pp. 272-79, 1993.
- [9] P. Dandeno et al., "Adaptation and validation of turbogenerator model parameters through on-line frequency response measurements", *IEEE Trans. Power Apparatus Syst.*, vol. 100, pp. 1656-64, 1981.
- [10] J. Melgoza et al., "An algebraic approach for identifying operating point dependent parameters of synchronous machines using orthogonal series expansions", *IEEE Trans. Energy Convers.*, vol. 16, pp. 92-8, 2001.
- [11] M. Arjona et al., "Parameter estimation of a synchronous generator using a sine cardinal perturbation and mixed stochastic-deterministic algorithms", *IEEE Trans. Ind. Electron.*, vol. 58, pp. 486-93, 2011.
- [12] H. Liu et al., "Finite element analysis of 1 MW high speed wound-rotor synchronous machine", *IEEE Trans. Magn.*, vol. 48, pp. 4650-53, 2012.
- [13] O. Laldin, S. Sudhoff and S. Pekarek, "An analytical design model for wound rotor synchronous machines", *IEEE Trans. Energy Convers.*, vol. 30, pp. 1299-09, 2015.
- [14] H. Yaghibi et al., "Application of radial basis neural networks in fault diagnosis of synchronous generator", *J. Iran. Assoc. Electr. Electron. Eng.*, vol. 10, pp. 23-36, 2013.
- [15] M. Karrari and O. Malik, "Nonlinear modeling of synchronous generators using wavelet transform-experimental results", *J. Iranian Assoc. Electr. Electron. Eng.*, vol. 1, pp. 24-30, 2004.
- [16] S. Nuzo et al., "Improved damper cage design for salient-pole synchronous generators", *IEEE Trans. Ind. Electron.*, vol. 64, pp. 1958-70, 2017.
- [17] Guide for Synchronous Generator Modeling Practices in Stability Analyzes, IEEE Std. 1110, 1991.
- [18] H. Gorginpour et al., "A novel rotor configuration for brushless doubly-fed induction generators", *IET Electr. Power Appl.*, vol. 7, pp. 106-115, 2013.
- [19] Z. Wu and O. Ojo, "Coupled-circuit-model simulation and airgap-field calculation of a dual-stator-winding induction machine", *IEEE Proc. Electr. Power Appl.*, vol. 153, pp. 387-400, 2006.
- [20] Z. Heidari, H. Gorginpour and M. Shahparasti, "Optimal electromagnetic-thermal design of a seven-phase induction motor for high-power variable-speed applications", *Sci. Iran.*, In-press, 2021.
- [21] M. Ojaghi and V. Bahari, "Rotor damping effects in dynamic modeling of three-phase synchronous machines under the stator interturn faults-winding function approach", *IEEE Trans. Ind. Appl.*, vol. 53, pp. 3020-28, 2017.
- [22] W. Xu et al., "Equivalent circuit derivation and performance analysis of a single-sided linear induction motor based on the winding function theory", *IEEE Trans. Veh. Tech.*, vol. 61, pp. 1515-25, 2012.
- [23] J. Pyrhonen, T. Jokinen and V. Hrabovcova, *Design of Rotating Electrical Machines*, 1<sup>st</sup> ed., 2008.
- [24] K. Murthy, *Computer-Aided Design of Electrical Machines*, 1<sup>st</sup> ed., BS Publications, 2008.